Journal of Taibah University for Science

ISSN: (Print) (Online) Journal homepage: https://www.tandfonline.com/loi/tusc20

A combined method for simulating MHD convection in square cavities through localized heating by method of line and penalty-artificial compressibility

Mohamed M. Mousa, Mohamed R. Ali & Wen-Xiu Ma

To cite this article: Mohamed M. Mousa, Mohamed R. Ali & Wen-Xiu Ma (2021) A combined method for simulating MHD convection in square cavities through localized heating by method of line and penalty-artificial compressibility, Journal of Taibah University for Science, 15:1, 208-217, DOI: 10.1080/16583655.2021.1951503

To link to this article: https://doi.org/10.1080/16583655.2021.1951503

Published online: 15 Jul 2021.

JOURNAL OF TAIBAH UNIVERSITY FOR SCIENCE
2021, VOL. 15, NO. 1, 208–217
https://doi.org/10.1080/16583655.2021.1951503

JTUSCI

Journal of Taibah University for Science

Taylor & Francis
Taylor & Francis Group

OPEN ACCESS Check for updates

A combined method for simulating MHD convection in square cavities through localized heating by method of line and penalty-artificial compressibility

Mohamed M. Mousa [a,b], Mohamed R. Ali [a] and Wen-Xiu Ma [c,d,e,f]

[a]Department of Basic Science, Faculty of Engineering at Benha, Benha University, Benha, Egypt; [b]Department of Mathematics, College of Sciences and Human Studies at Howtat Sudair, Majmaah University, Majmaah, Saudi Arabia; [c]Department of Mathematics, Zhejiang Normal University, Jinhua, Zhejiang, People's Republic of China; [d]Department of Mathematics, King Abdulaziz University, Jeddah, Saudi Arabia; [e]Department of Mathematics and Statistics, University of South Florida, Tampa, FL, USA; [f]School of Mathematical and Statistical Sciences, North-West University, Mmabatho, South Africa

ABSTRACT

A new combined technique is developed for studying free convection of magnetohydrodynamic unsteady incompressible flow in a square cavity that partially heated from lower wall and regular cooling from lateral walls. Convection has been studied for several lengths of heat source, Hartman and the Rayleigh numbers. The local and average Nusselt numbers are calculated and presented graphically along the heat source portion. The proposed technique is a combination of the method of lines (MOL) and a developed penalty-artificial compressibility technique (PACT). Unsteady penalty compressibility governing equations are used instead of solving steady-state balances. The penalty and artificial compressibility factors are estimated using a deduced stability restriction. The validation of the MOL-PACT is verified by comparing the current data with other numerical and experimental ones existing in the literature. The proposed technique provides a new choice through the investigation of MHD mass and heat transfer.

ARTICLE HISTORY
Received 5 August 2020
Revised 8 February 2021
Accepted 19 April 2021

KEYWORDS
MHD free convection; method of lines; penalty method; artificial compressibility technique; heat transfer

1. Introduction

Free convection, induced by internal heat generation, in square cavities has received significant attention because of its many applications in geophysics and energy related to engineering problems. Indeed, natural convection in closed enclosures with various heated boundaries is a model of various engineering applications like the safety and operation of a nuclear reactor and convective heat transfer related to electronic cooling devices. In some practical applications such as metal casting, the crystal growth in a fluid, the extractions of geothermal energy and the fusion reactors, the free convection has occurred within the magnetic field effect.

Analysis of the literature reveals comparatively huge attention in the convective phenomenon study in a square and rectangular cavity heated from the lower wall and subjected to dissimilar isothermal conditions. As example, and not as a limitation, Sharma et al. [1] investigated the turbulent free convection in a square cavity containing a localized heater at a lower wall and identical cooling at vertical sidewalls. Their research models the situation of the unintended heat generation resulted from a fire in an isolated body of an electronic components cabin or a nuclear reactor. In [2], the natural convection in a rectangle cavity which was partly heated from the lower wall and equivalently cooled at the vertical sidewalls has been numerically investigated. Calcagni et al. [3] experimentally and numerically investigated natural convection and heat transfer in a square cavity that happened by a heater positioned on the bottom wall and cooled from the sidewalls. In this research, they examined how the transferring of heat grows in the cavity due to the increase of the heat source length. A systematic numerical study of 2D steady laminar free convection in a rectangle cavity due to localized heaters of various walls thermal conditions is considered by Deng et al. [4]. Yigit et al. [5] numerically studied the steady laminar free convection of power-law fluids in a square cavity containing a partial heater at the bottom wall and identical cooling at sidewalls by ANSYS-FLUENT solver. Recently, many researchers have investigated many problems related to MHD free convection. In [6], Colak et al. have examined magnetohydrodynamic mixed convection in a chamfered lid-driven enclosure containing a fractional heater. Sajjadi et al. [7] have done a 3D mesoscopic simulation of magnetohydrodynamic free convection in a cubic enclosure using the Lattice-Boltzmann method and with two multi relaxation time models. In [8],

CONTACT Mohamed R. Ali mohamed.reda@bhit.bu.edu.eg Department of Basic Science, Faculty of Engineering at Benha, Benha University, 13512, Egypt; Department of Mathematics, Zhejiang Normal University, Jinhua, Zhejiang 321004, People's Republic of China

Usman et al. have investigated the magnetohydrodynamic heat and mass transfer flow inside a square enclosure heated from the top wall and equipped with cold and heated square obstacles. Sivaraj and Sheremet [9] investigated the free convection in a tending porous enclosure containing heated compact obstacle located at the centre in presence of an applied magnetic field of diverse orientations. Zhang et al. [10] studied the MHD free convection in square and cube cavities in presence of the effects of thermal radiation using the spectral collocation-artificial compressibility method (ACM). In [11], Shahid and Tunç have obtained exact expressions of temperature and velocity of an elastoviscous magnetohydrodynamic fluid slipping past an unbounded upright channel with a vacillating temperature.

Method of lines [12–16] as modified (G'/G)-expansion method [17,18] is one of the efficient and accurate numerical methods that have been handled successfully to solve many partial differential equations (PDEs) with high accuracy. The idea of the MOL is summarized in reducing the given partial differential equations to a system of ordinary differential equations (ODEs) in the time by discretization of space variables and spatial derivatives using finite difference schemes. Then the resultant ODEs system can be solved using a suitable ODE solver like the 4th order Runge–Kutta method (RK4). As a global approach, the MOL is used in this work for solving PDEs of Navier–Stokes that describes the flow of incompressible fluids. In order to utilize this explicit method in solving such PDEs, the ellipticity in Navier–Stokes equations must be removed. The leading method to achieve this is using the penalty method [19], which was received significant attraction in the last years, especially in the finite element and free convection community [20–23]. The idea of this technique is based on eliminating the pressure variable (p) in the momentum conservation equations with the aid of a mass conservation equation (continuity equation) that will be used as a restriction. In the penalty method, the errors in the divergence of velocity are transferred to the boundaries [24]. An alternative related technique is the artificial compressibility technique (ACT) [25–29], in which the deviations from incompressibility determine $\partial p/\partial t$ rather than p itself. Also, the ACT diffuses errors in velocity divergence. The penalty method and ACT converge to the Navier–Stokes equations in the limit as their parameters approach to infinity [30].

Therefore, we try to utilize a combination between MOL, penalty method and ACT for the purpose of spatial discretizing of PDEs of unsteady penalty-artificial compressibility and present the MOL-PACT for solving PDEs governing natural convection of MHD laminar incompressible fluid in a square cavity with a partial heater at the bottom wall and cooled from sidewalls. Optimal values of penalty and artificial compressibility parameters are calculated using a deduced stability condition. The validation of the developed technique is tested by comparing the obtained results with other experimental and numerical results existing in the literature as well. As we will see in the model validation section, an excellent agreement between the obtained results and the results that exciting in the literature [1,2], when neglecting the magnetic field effect, is achieved although the simplicity of the method. This can be considered one of the advantages and benefits of the proposed method.

2. Mathematical and physical model

Suppose the motion of viscous fluid in a square encloser of length Las shown in Figure 1. The heat source of length l is centrally positioned on the lower wall and varied from 0.2 to 0.8 of L. The $\frac{l}{L}$ is termed as ε (dimensionless heated length piece). The upper wall and the unheated piece of the lower wall are adiabatic; however, the vertical sidewalls are maintained at a fixed temperature T_c and the heated piece of the lower wall is at a temperature T_h. The change in the fluid density with temperature is combined using the Boussinesq approximation. The encloser is subjected to a horizontal uniform magnetic field with a magnitude B_0, [31] while the brought magnetic field is neglected being small as compared to B_0. Enclosure walls are supposed to be electrically deposed with no Hall impacts. Under these hypotheses, the transient form of continuity, energy and momentum equations can be obtained from [21] by adding the term which represents the magnetic field effect or from [32] by removing the term which represents the medium permeability effect,

$$\frac{\partial u}{\partial x}+\frac{\partial v}{\partial y}=0, \tag{1}$$

$$\frac{\partial u}{\partial t}+u\frac{\partial u}{\partial x}+v\frac{\partial u}{\partial y}=-\frac{1}{\rho}\frac{\partial p}{\partial x}+\nu\left(\frac{\partial^2 u}{\partial x^2}+\frac{\partial^2 u}{\partial y^2}\right), \tag{2}$$

$$\frac{\partial v}{\partial t}+\frac{\partial v}{\partial x}+u\frac{\partial v}{\partial y}=-\frac{1}{\rho}\frac{\partial p}{\partial y}+\nu\left(\frac{\partial^2 v}{\partial x^2}+\frac{\partial^2 v}{\partial y^2}\right) -\frac{\sigma B_0^2}{\rho}v+g\beta\left(T-T_c\right), \tag{3}$$

$$\frac{\partial T}{\partial t}+u\frac{\partial T}{\partial x}+v\frac{\partial T}{\partial y}=\alpha\left(\frac{\partial^2 T}{\partial x^2}+\frac{\partial^2 T}{\partial y^2}\right), \tag{4}$$

wherever u and v are the velocities in x and y directions sequentially, p is the pressure, ρ is the density, β is the coefficient of thermic expansion, α is the thermic diffusivity, ν is the viscosity, σ is the conductivity and g is the gravity acceleration.

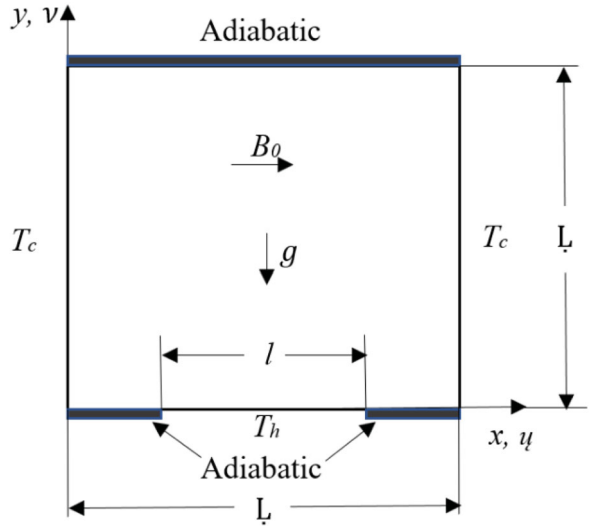

Figure 1. Geometry and physical model.

The boundary conditions (BCs) for our case are:

- vertical sidewalls walls: $u = v = 0, T = T_c$,
- lower wall: $u = v = 0, \frac{\partial T}{\partial y} = 0$, at $0 \le x \le \left(\frac{1-\varepsilon}{2}\right) L$ and $\left(\frac{1-\varepsilon}{2}\right) L \le x \le L$, $T = T_h$, for $\left(\frac{1-\varepsilon}{2}\right) L \le x \le \left(\frac{1+\varepsilon}{2}\right) L$,
- upper wall: $u = v = 0, \frac{\partial T}{\partial y} = 0$.

Substituting the nondimensional variables:

$$\xi = \frac{x}{L}, Y = \frac{y}{L}, \quad \tau = \frac{\alpha t}{L^2}, \quad \grave{U} = \frac{uL}{\alpha}, \quad \mathcal{V} = \frac{vL}{\alpha},$$
$$P = \frac{\mathcal{P}L^2}{\rho\alpha^2}, \quad \vartheta = \frac{T - T_c}{T_h - T_c}, \quad Pr = \frac{\nu}{\alpha},$$
$$Ra = \frac{g\beta L^3 (T_h - T_c)}{\alpha\nu}, \quad Ha = B_0 L\sqrt{\frac{\sigma}{\rho\nu}}.$$

into Equations (1)–(4) yields dimensionless equations

$$\frac{\partial \grave{U}}{\partial \chi} + \frac{\partial \mathcal{V}}{\partial Y} = 0, \tag{5}$$

$$\frac{\partial \grave{U}}{\partial \tau} + \grave{U}\frac{\partial \grave{U}}{\partial \chi} + \mathcal{V}\frac{\partial \grave{U}}{\partial Y} = -\frac{\partial P}{\partial \chi} + Pr\left(\frac{\partial^2 \grave{U}}{\partial \chi^2} + \frac{\partial^2 \grave{U}}{\partial Y^2}\right), \tag{6}$$

$$\frac{\partial \mathcal{V}}{\partial \tau} + \grave{U}\frac{\partial \grave{U}}{\partial \chi} + \mathcal{V}\frac{\partial \mathcal{V}}{\partial Y} = -\frac{\partial P}{\partial Y} + Pr\left(\frac{\partial^2 \mathcal{V}}{\partial \chi^2} + \frac{\partial^2 \mathcal{V}}{\partial Y^2}\right) - P_r Ha^2 \mathcal{V} + P_r R_a \vartheta, \tag{7}$$

$$\frac{\partial \vartheta}{\partial \tau} + \grave{U}\frac{\partial \vartheta}{\partial \chi} + \mathcal{V}\frac{\partial \vartheta}{\partial Y} = \frac{\partial^2 \vartheta}{\partial \chi^2} + \frac{\partial^2 \vartheta}{\partial Y^2}. \tag{8}$$

And hence the BCs are reduced to:

- vertical sidewalls walls: $\grave{U} = \mathcal{V} = \vartheta = 0$,
- lower wall: $\grave{U} = \mathcal{V} = 0, \frac{\partial \vartheta}{\partial Y} = 0$, for $0 \le \chi \le \left(\frac{1-\varepsilon}{2}\right)$ and $\left(\frac{1+\varepsilon}{2}\right) \le \chi \le 1$,

$$\vartheta = 1, \text{ for } \left(\frac{1-\varepsilon}{2}\right) \le \chi \le \left(\frac{1+\varepsilon}{2}\right),$$

- upper wall: $\grave{U} = \mathcal{V} = \frac{\partial \vartheta}{\partial Y} = 0$.

Here $\grave{U}, \mathcal{V}, P$ and ϑ are the nondimensional velocities components, pressure and temperature, respectively. The parameters P_r, R_a and H_a represent the Prandtl, Rayleigh and Hartman numbers, respectively. The rate of the heat transfer through the heated portion of the lower wall can be quantified using the averaged Nusselt symbol Nu_{avg} and local Nusselt symbol ($Nu(\chi)$) that given by, respectively,

$$Nu_{\text{avg.}} = \int_{\frac{1-\varepsilon}{2}}^{\frac{1+\varepsilon}{2}} Nu\,(\chi)\; d\chi, \tag{9}$$

$$Nu(\chi) = -\left.\frac{\partial \vartheta}{\partial Y}\right|_{Y=0}. \tag{10}$$

The motion of the fluid can be presented by the stream function ψ that can be perceived from the velocities $\grave{U}$ and $\mathcal{V}$ as:

$$\grave{U} = \frac{\partial \psi}{\partial Y}, \mathcal{V} = -\frac{\partial \psi}{\partial \chi}. \tag{11}$$

Equation (11) leads to the following Poisson's equation, for obtaining the stream function ψ.

$$\frac{\partial^2 \psi}{\partial \chi^2} + \frac{\partial^2 \psi}{\partial Y^2} = \frac{\partial \grave{U}}{\partial Y} - \frac{\partial \mathcal{V}}{\partial \chi}. \tag{12}$$

Because of a nonslip condition, $\psi = 0$ is considered at all boundaries of the cavity.

3. Mathematical formulation and numerical procedure

3.1. Penalty-artificial compressibility technique (PACT)

Based on the penalty method and the artificial compressibility technique, instead of continuity equation (5), we present the following penalty-artificial compressibility equation

$$\frac{\partial P}{\partial \tau} = -c^2\left(\frac{\partial \grave{U}}{\partial \chi} + \frac{\partial \mathcal{V}}{\partial Y}\right) - b\frac{\partial}{\partial \tau}\left(\frac{\partial \grave{U}}{\partial \chi} + \frac{\partial \mathcal{V}}{\partial Y}\right), \tag{13}$$

where the constant c represents the artificial compressibility parameter and b represents the penalty parameter. When $c = 0$, Equation (13) reduces to the time derivative of the penalty equation, while if $b = 0$, it reduces to the artificial compressibility equation. Due to

the choice of no-slip conditions at all boundaries, $P = 0$ is at all walls of the cavity. Initial conditions of $\grave{U}, \mathcal{V}, \vartheta$ and P at time $\tau = 0$ are selected to be identical to the same appreciation of the closest boundary. To estimate suitable appreciation of b and c that are needed to solve the system of Equations (6)–(8) and (13), firstly we construct the MOL finite difference scheme and then we apply a suitable stability technique as the conventional linearized Fourier stability analysis.

3.2. MOL and stability analysis

As indicated by the MOL, the coordinate χ and Y in the system of Equations (6)–(8) and (13) is discretized with $N \times N$ regularly 2D spaced grid points where $\chi_i = \chi_{i-1} + \Delta\chi, Y_j = Y_{j-1} + \Delta Y, \chi_0 = Y_0 = 0, \chi_N = Y_N = 1$, $i, j = 1, 2, \ldots, N$ and $\Delta\chi = \Delta Y = 1/N$. Central finite difference scheme with a second-order accuracy used to approximate the first and second derivatives corresponding to the spatial variables χ and Y at each grid point (χ_i, Y_j) for $i, j = 2, 3, \ldots, N-1$.Then the 4th Runge–Kutta technique is utilized as a time integrator to solve the ODEs system upon the pre-described initial conditions with an appropriate step time $\Delta\tau$. The central first- and second-ordered finite difference operators regarding χ and Y are defined as:

$$D_{1x}[F_{i,j}] = \frac{(F_{i+1,j} - F_{i-1,j})}{2\Delta\chi},$$

$$D_{1y}[F_{i,j}] = \frac{(F_{i,j+1} - F_{i,j-1})}{2\Delta Y},$$

$$D_{2x}[F_{i,j}] = \frac{(F_{i+1,j} - 2F_{i,j} + F_{i-1,j})}{\Delta\chi^2} \text{ and}$$

$$D_{2y}[F_{i,j}] = \frac{(F_{i,j+1} - 2F_{i,j} + F_{i,j-1})}{\Delta Y^2}.$$

In order to drive a stability condition needed to estimate the constants b and c, we write the finite difference scheme of Equations (6)–(8) and (13) in a forward Euler explicit representation with respect to time τ, as

$$\begin{aligned}\grave{U}_{i,j}^{k+1} &= \grave{U}_{i,j}^{k} + \Delta\tau(-\grave{U}_{i,j}^{k} D_{1x}[\grave{U}_{i,j}^{k}] - \mathcal{V}_{i,j}^{k} D_{1y}[\grave{U}_{i,j}^{k}] \\ &\quad - D_{1x}[P_{i,j}^{k}] + P_r(D_{2x}[\grave{U}_{i,j}^{k}] + D_{2y}[\grave{U}_{i,j}^{k}])), \end{aligned} \tag{14}$$

$$\begin{aligned}\mathcal{V}_{i,j}^{k+1} &= \mathcal{V}_{i,j}^{k} + \Delta\tau(-\grave{U}_{i,j}^{k} D_{1x}[\mathcal{V}_{i,j}^{k}] \\ &\quad - \mathcal{V}_{i,j}^{k} D_{1y}[\mathcal{V}_{i,j}^{k}] - D_{1y}[P_{i,j}^{k}] \\ &\quad - P_r Ha^2[\mathcal{V}_{i,j}^{k}] + P_r R_a \vartheta_{i,j}^{k} \\ &\quad + P_r(D_{2x}[\mathcal{V}_{i,j}^{k}] + D_{2y}[\mathcal{V}_{i,j}^{k}]), \end{aligned} \tag{15}$$

$$\begin{aligned}\vartheta_{i,j}^{k+1} &= \vartheta_{i,j}^{k} + \Delta\tau(-\grave{U}_{i,j}^{k} D_{1x}[\vartheta_{i,j}^{k}] - \mathcal{V}_{i,j}^{k} D_{1y}[\vartheta_{i,j}^{k}] \\ &\quad + D_{2x}[\vartheta_{i,j}^{k}] + D_{2y}[\vartheta_{i,j}^{k}]), \end{aligned} \tag{16}$$

$$\begin{aligned}P_{i,j}^{k+1} &= P_{i,j}^{k} - c^2\Delta\tau(D_{1x}[\grave{U}_{i,j}^{k}] + D_{1y}[\mathcal{V}_{i,j}^{k}]) \\ &\quad - b(D_{1x}[\grave{U}_{i,j}^{k}] - D_{1x}[\grave{U}_{i,j}^{k-1}] + D_{1y}[\mathcal{V}_{i,j}^{k}] \\ &\quad - D_{1y}[\mathcal{V}_{i,j}^{k-1}]), \end{aligned} \tag{17}$$

where k is the time level.

Ignoring the convection terms in the present finite difference scheme and applying a linearized von Neumann stability analysis [33] yield the following stability condition [34,35]:

$$\Delta\tau\left(\frac{1}{\Delta\chi^2} + \frac{1}{\Delta Y^2}\right)(c^2\Delta\tau + 2(b + Pr)) < 1. \tag{18}$$

Setting $\Delta^2 = \left(\frac{1}{\Delta\chi^2} + \frac{1}{\Delta Y^2}\right)^{-1}$, and defining a mixture ratio $M = \frac{c^2\Delta\tau}{2(b+P_r)}$, the stability restriction (18) can be written as

$$\frac{2\Delta\tau}{\Delta^2}(b + P_r)(M + 1) < 1. \tag{19}$$

The values $M = 0$ and $M = \infty$ correspond to the pure penalty technique and ACT, respectively, while values near $M = 1$ correspond to a roughly equal mixture of the two techniques. In order to estimate a value of the parameter b form inequality (19), we introduce a safety factor f where $0 < f < 1$. Thus, we can obtain b and c^2 that are safely consistent with stability condition as

$$b = \frac{f\Delta^2}{2\Delta\tau(M + 1)} - Pr, \tag{20}$$

$$c^2 = \frac{fM\Delta^2}{\Delta\tau^2(M + 1)}. \tag{21}$$

From the relations (20) and (21), that satisfying the stability condition, one can estimate the values of b and c^2 for a given grid by setting arbitrary values of Prandtl number P_r, mixture ratio M, safety factor f and selecting a small value of $\Delta\tau$.

All results that will be discussed in Section 5 are computed using a grid of size 40×40 points for $P_r = 0.71$ (air), $M = 1, f = 0.8$ and $\Delta\tau = 10^{-5}$. These arbitrary values give that $b = 5.54$ and $c^2 = 1.25 \times 10^6$. The optimal value of the mixture ratio M is selected upon analysing maximum absolute deviations (relative error) in the continuity equation for several values of M ranging from $M = 10^{-4}$ to $M = 10^4$. This analysis is not shown here. A detailed analysis of choosing the optimal value of the mixture ratio M and the safety factor f can be found in [34,35].

The grid of size 40×40 is decided upon the next grid independence study. RK4 technique is used as an integrator of the resulting ODEs system, instead of Euler technique, for the purpose of obtaining more accurate results. The stream function ψ is obtained by applying the successive over-relaxation technique, with suitable accuracy, to the system of linear algebraic equations resulted from the following equation

$$D_{2x}[\psi_{i,j}^{k}] + D_{2y}[\psi_{i,j}^{k}] = D_{1y}[\grave{U}_{i,j}^{k}] - D_{1x}[\mathcal{V}_{i,j}^{k}]. \tag{22}$$

The steady-state solution is checked by employing the following condition

$$\sum_{i,j} |\Phi_{i,j}^{k+1} - \Phi_{i,j}^{k}| < 10^{-5}, \tag{23}$$

where Φ stands for $\grave{U}, \mathcal{V}, \vartheta, P$ or ψ.

Table 1. Grid independence study when $R_a = 10^6, H_a = 0, \varepsilon = 0.2$ and $\varepsilon = 0.8$.

		$\varepsilon = 0.2$		$\varepsilon = 0.8$	
Grid	$N \times N$	$Nu_{avg.}$	% Change	$Nu_{avg.}$	% Change
G1	20×20	3.517	–	10.912	–
G2	40×40	3.648	3.59	11.278	3.25
G3	80×80	3.675	0.73	11.322	0.39

Table 2. Comparison of $Nu_{avg.}$ of the present work with experimental and numerical values of [1–3] when $H_a = 0, \varepsilon = 0.8$ for various values of R_a.

	The average Nusselt number ($Nu_{avg.}$)			
R_a	Present work	Sharma et al. [1]	Aydin and Yang [2]	Calcagni et al. [3]
10^4	3.750	3.76	3.9	4.0
10^5	6.142	6.15	6.2	6.3
10^6	11.278	12.84	11.3	12.0

4. Study of grid independency and model validation

4.1. Study of grid independency

Calculations have been gotten on three meshes to test the grid independency of the numerical scheme: G1 : 20×20, G2 : 40×40 and G3 : 80×80. The grid independence study is done for the average Nusselt number along with the heated piece of the lower wall when $R_a = 10^6, H_a = 0, \varepsilon = 0.2$ and $\varepsilon = 0.8$. The results of the grid study for the three grids are presented in Table 1.

As shown in Table 1, the variance in $Nu_{avg.}$ between the grids G1 and G2 is 3.59% for $\varepsilon = 0.2$ and 3.25% for $\varepsilon = 0.8$, while between G2 and G3 is only 0.73% for $\varepsilon = 0.2$ and 0.39% for $\varepsilon = 0.8$. So, a grid pattern of G2 is considered in all study computations.

4.2. Validation of the model

Through the objective of consequences validation, the results got from the present work are discussed with the experimental and numerical ones of Sharma et al. [1], Aydin and Yang [2] and Calcagni et al. [3] with identical boundary conditions and R_a values in absence of the magnetic field effect, i.e. $H_a = 0$. The average Nusselt number at the heated portion of the lower wall of dimensionless length $\varepsilon = 0.8$ are discussed in Table 2, with the obtained results. It can be noted that the agreement is good. For further results validation, some of the obtained results are validated against ones obtained in [2,3] when $H_a = 0$ as shown in Figure 2. The upper row of Figure 2 contains plots of temperature contours when considering $\varepsilon = 0.8$ at $R_a = 10^5$, while the lower row contains plots of the Nusselt number variations along the heated piece of the lower wall with the Rayleigh symbol for all values of ε. From Figure 2, one can state that, a good agreement is detected between present consequences and numerical experimental results existing in [2,3]. This agreement is enough to ensure the validation and accuracy of the present computational scheme.

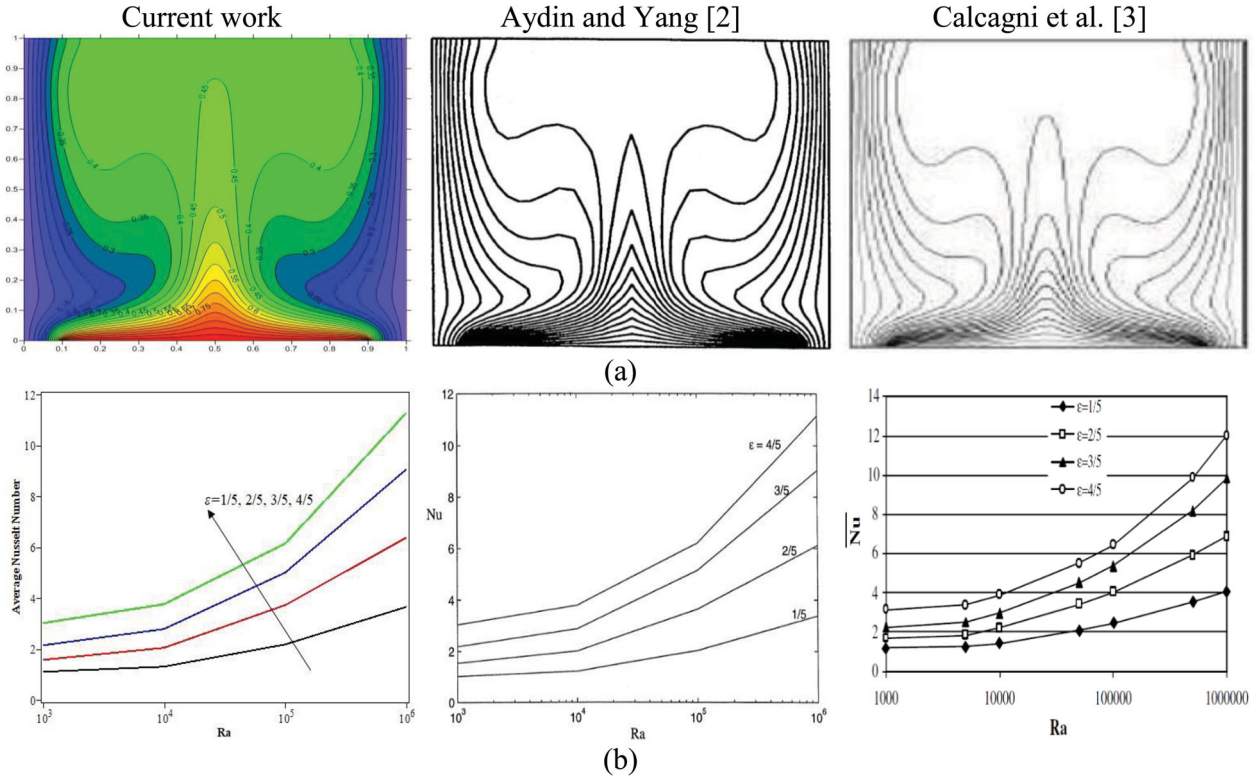

Figure 2. A comparison between present results and numerical/experimental results in [2,3] (a) isotherms when $R_a = 10^5, \varepsilon = 0.8$ and (b) $Nu_{avg.}$ versus R_a for various values of ε when $H_a = 0$.

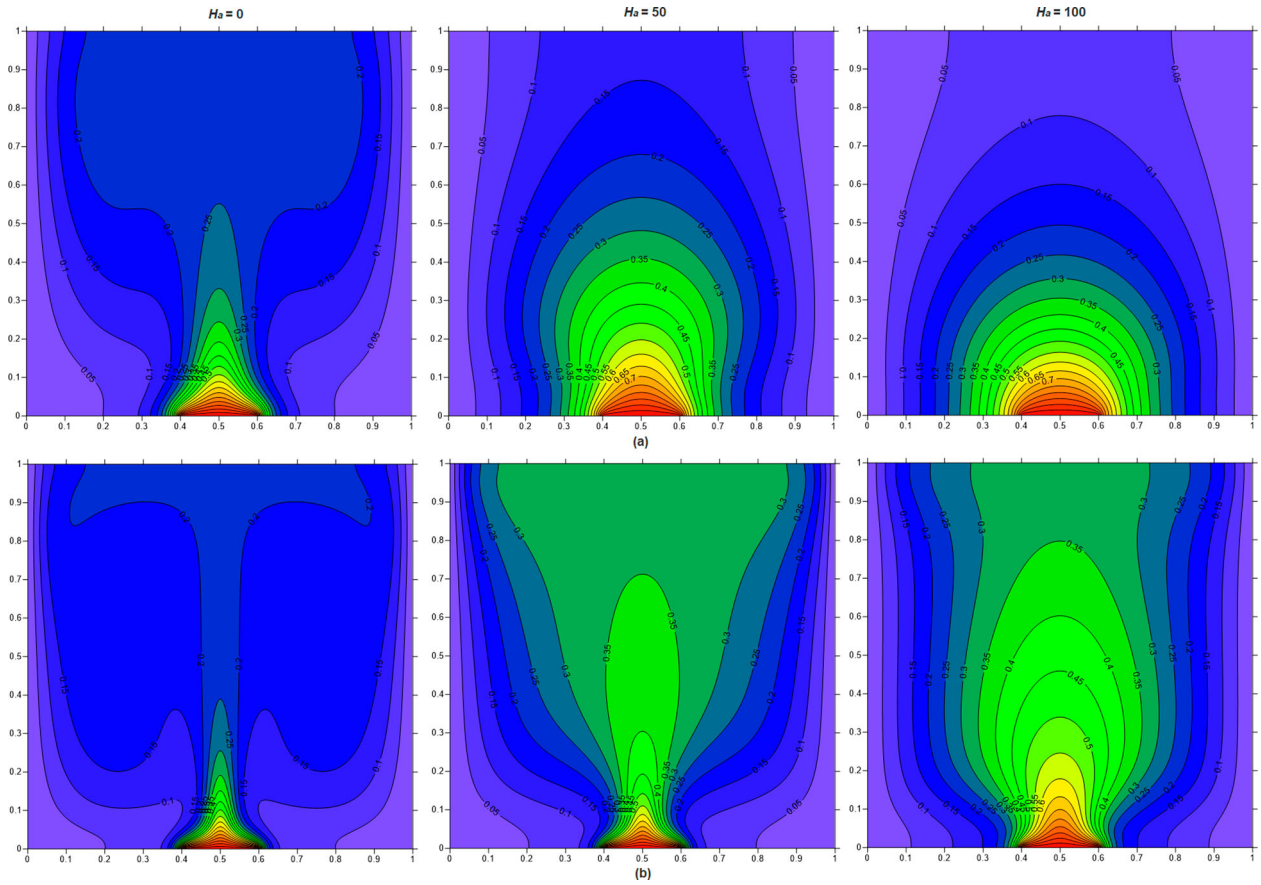

Figure 3. Isotherms at $\varepsilon = 0.2$ and different values of H_a, (a) when $R_a = 10^5$ and (b) when $R_a = 10^6$.

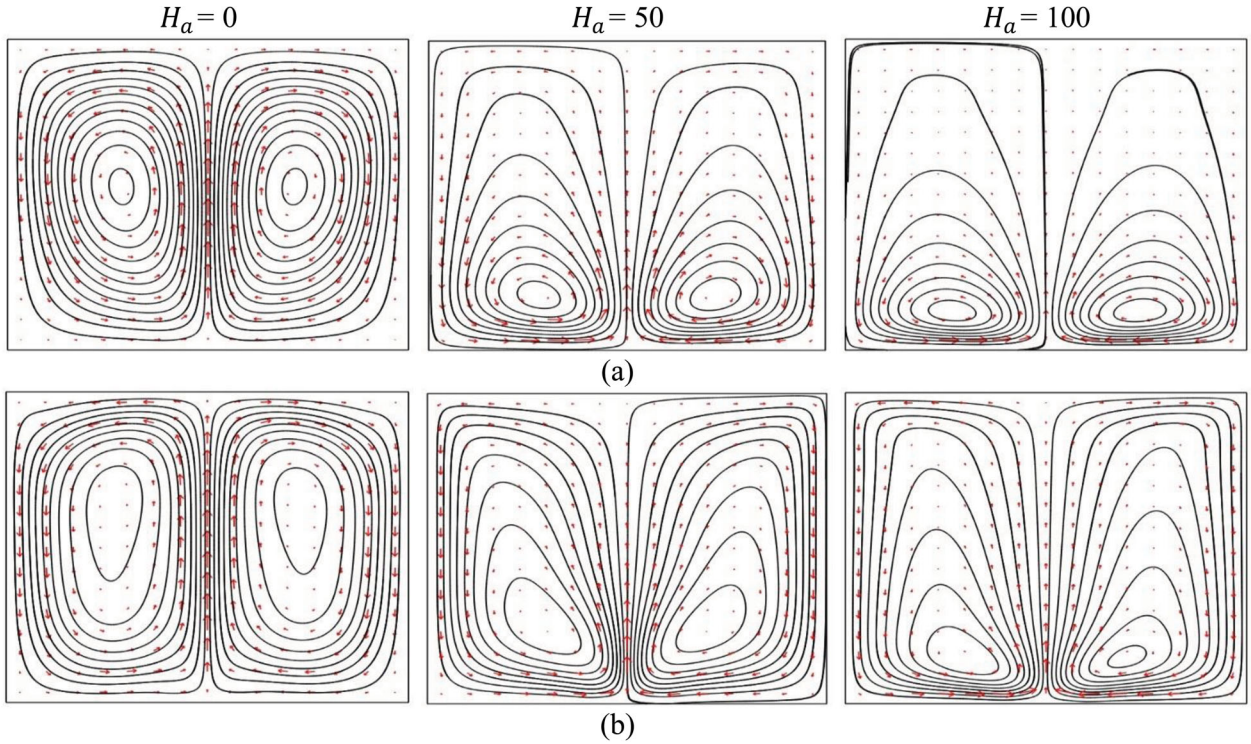

Figure 4. Streamlines at $\varepsilon = 0.2$ and different values of H_a, (a) when $R_a = 10^5$ and (b) when $R_a = 10^6$.

5. Results and discussions

Here, we discuss the results of the MOL-PACT numerical solution for simulating 2D steady laminar flow under the effects of MHD inside a square enclosure with a partially heating from the lower wall and symmetrical cooling from vertical sidewalls with an isolated upper side. The results are investigated by obtaining isotherms, streamlines, local and average Nusselt numbers for several

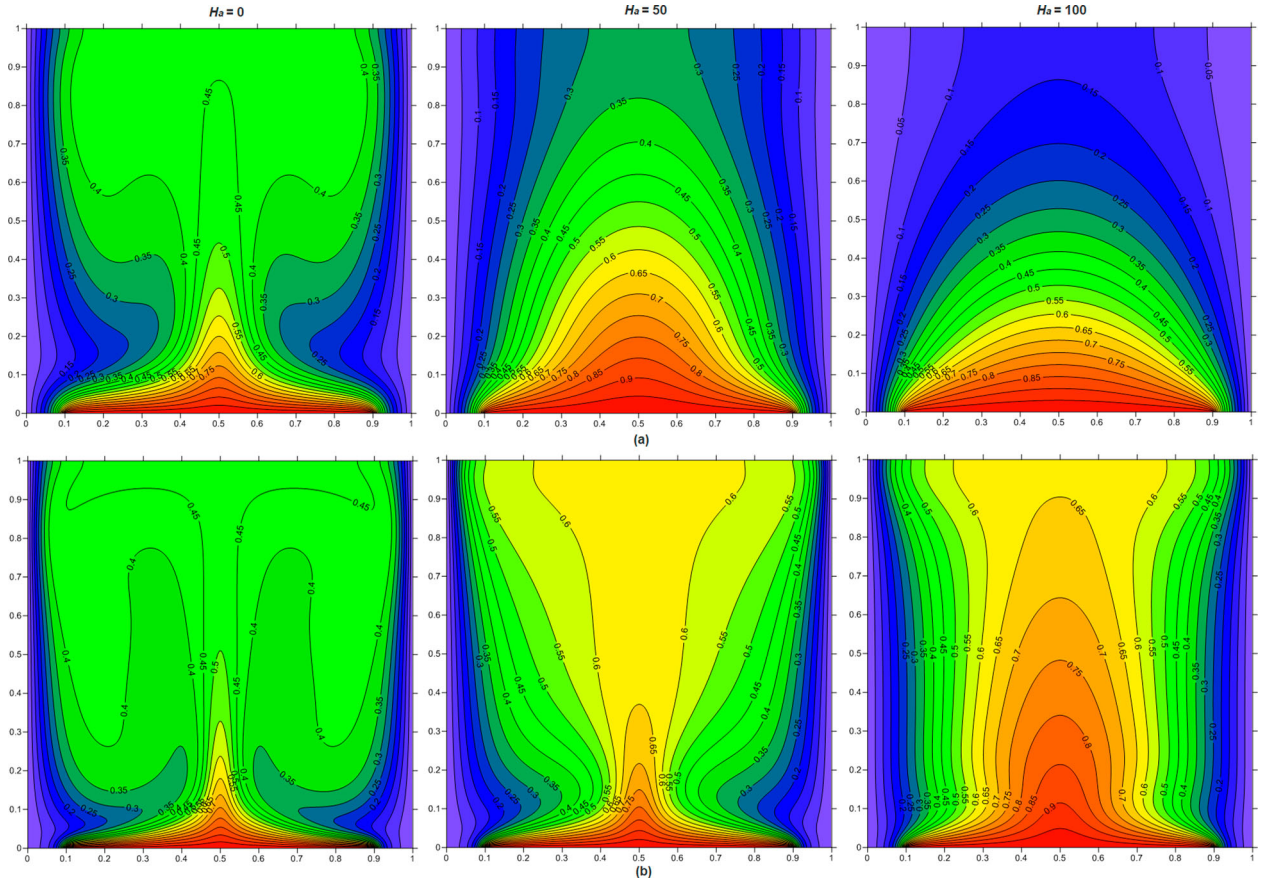

Figure 5. Isotherms at $\varepsilon = 0.8$ and different values of H_a, (a) when $R_a = 10^5$ and (b) when $R_a = 10^6$.

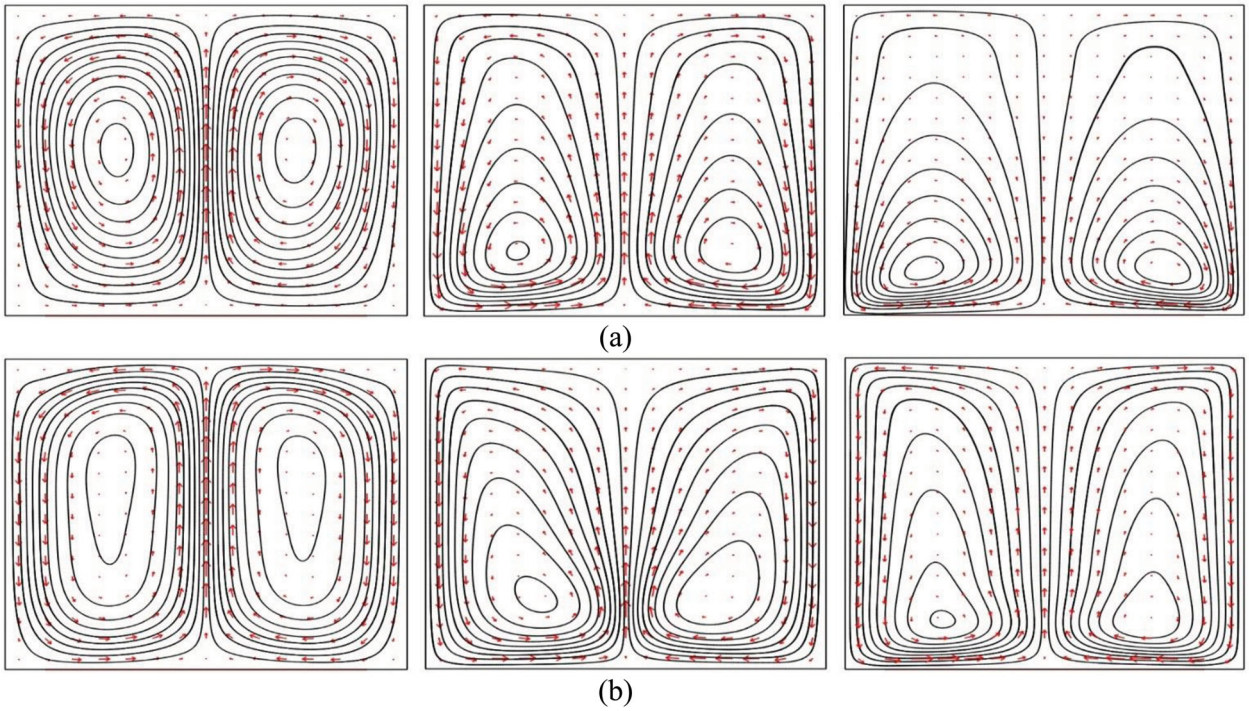

Figure 6. Streamlines at $\varepsilon = 0.8$ and different values of H_a, (a) when $R_a = 10^5$ and (b) when $R_a = 10^6$.

values of $R_a(10^3$ to $10^6)$, $H_a(0$ to $100)$ and $\varepsilon(0.2$ to $0.8)$ while P_r is remained fixed at 0.71. The simulation is done to study the impact of Hartman number, Rayleigh number, and dimensionless heated length part on fluid stream function, temperature distribution (isotherms) and rate of heat transfer.

Figures 3–6 depict the isotherms and streamlines in the cavity for various values of R_a, H_a and ε. From Figures 3 and 5; it can be illustrated that as the Rayleigh number increases, the thermal layers will be thinner causing increased heat transfer and the gradients of temperature become high near the heated bottom side.

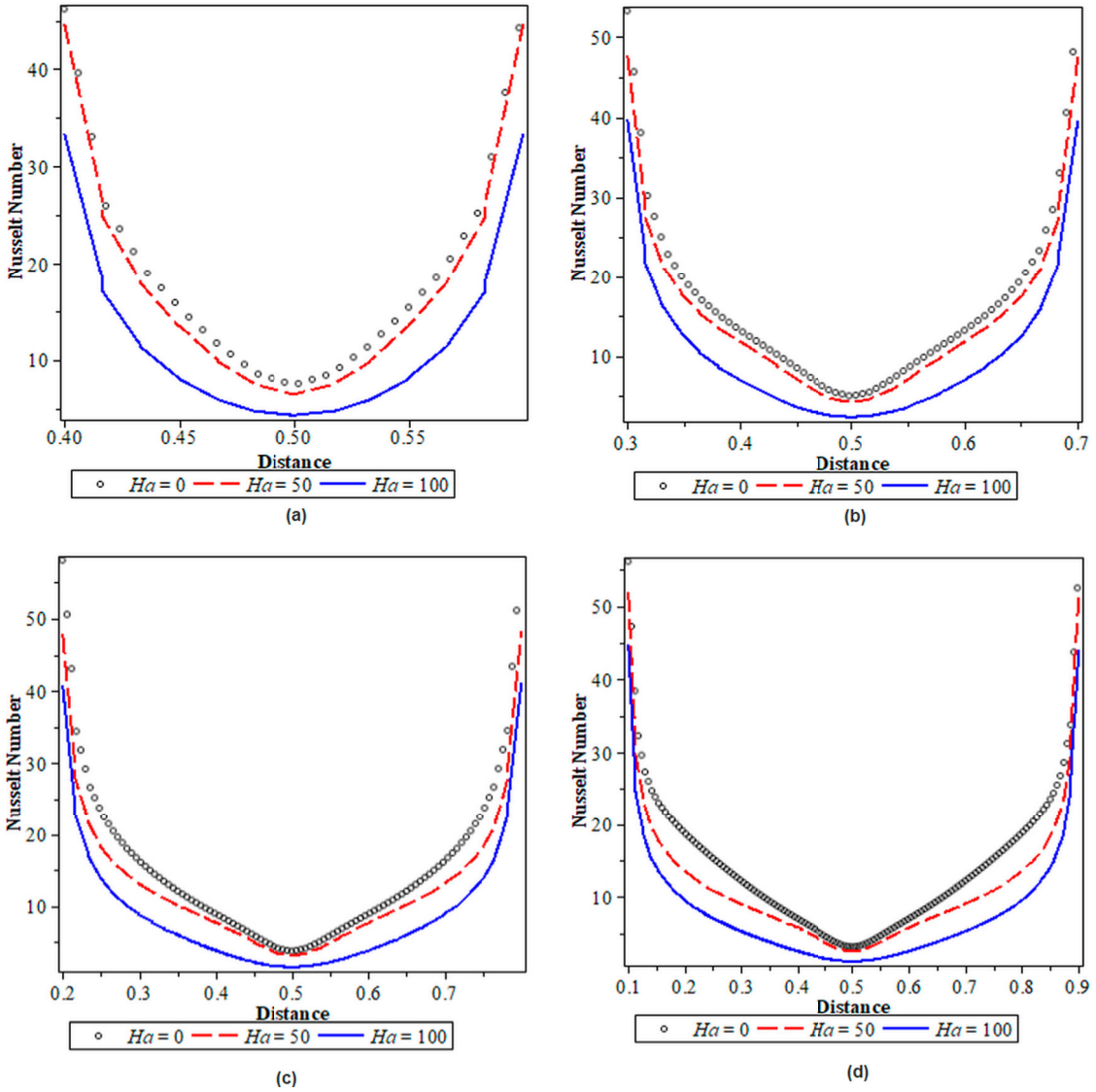

Figure 7. Variations of Nusselt number along the heated part of the lower wall for various Hartman numbers at $R_a = 10^6$, (a) $\varepsilon = 0.2$, (b) $\varepsilon = 0.4$, (c) $\varepsilon = 0.6$ and (d) $\varepsilon = 0.8$.

Moreover, temperature distribution will be stratified and the stratification degree grows with the growing of R_a. The larger R_a means further fluid circulation, and so, further heat is added to the fluid to upsurge the convection of the fluid. The Hartmann number presents a measure of the magnetic field effect on thermal free convection. The amount of the heat transfer dramatically reduces with the growth of H_a due to the fact, that the magnetic field tends to resist the fluid motion inside the cavity as shown in Figures 3 and 5.

From Figures 4 and 6 when $H_a = 0$, one can detect that the growing of the Rayleigh number will grow the strength of the circulation inside the cavity and make the cores of the vortex's cells move upward as concluded in [2]. On other hand as H_a increases, the main recirculation cell moves downward because of the magnetic field strength effect. For a fixed H_a, the streamlines remain almost similar but the boundary layer near the midpoint of the bottom wall becomes slightly compressed.

To show the impacts of R_a, H_a and ε on the heat transfer rate inside the cavity, it is important to visualize the local and average Nusselt number. Figure 7 represents Nu along heated part of the lower wall for various values of H_a and ε at $R_a = 10^6$. For a fixed ε, increasing H_a resists the fluid convection. Moreover, growing ε for a fixed value of H_a produces a raise in heat transfer. These outcomes can be obviously illustrated under the temperature distribution demonstrated in Figures 3 and 5. Figure 8 illustrates the variations of $Nu_{\text{avg.}}$along heated part of the lower wall versus R_a for all values of ε, $H_a = 0$ and $H_a = 100$. This figure summarizes the effects of R_a, H_a and ε on the heat transfer rate inside the fluid. It can be shown that the rate of heat transfer enhances by increasing Rayleigh number and dimensionless heated length, while it reduces by decreasing the magnetic field parameter H_a. When $H_a = 0$, the shown results in Figure 8, are consistent with the results obtained in [2,3]. On other hand, when $H_a = 100$, the values of $Nu_{\text{avg.}}$ remain approximately

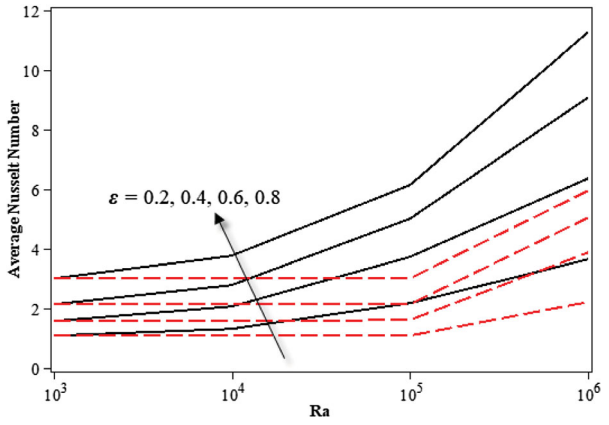

Figure 8. Average Nusselt number variation over the heated part of the lower wall versus the Rayleigh number for all values of ε, at $H_a = 0$ (solid line) and $H_a = 100$ (dash line).

constant till $R_a = 10^5$ then begin to increase when $R_a = 10^6$.

6. Conclusion

In this work, the mixed technique MOL-PACT is developed for modelling MHD laminar flows and heat transfer problems. Although the developed technique is proposed to generate accurate transient solutions, it is also applicable to calculate steady-state solutions. The developed technique is combining hyperbolic and parabolic nature to get improved convergence behaviour than either one alone may offer. The penalty and artificial compressibility parameters that consistent with the deduced stability restriction are estimated.

As an example, to verify the efficiency of the MOL-PACT, the technique is used to model the MHD free convection in a square cavity with a localized heating. The simulation is done to investigate the influence of magnetic field parameter, Rayleigh number and heated source length on the flow, isotherms and rate of the heat transfer. The main conclusions of the simulation are as follows. The flow and temperature distribution are symmetrical around mid-length of the cavity because of the symmetry nature of considered conditions. By increasing the Rayleigh number, the flow recirculation growths, and the cores of the vortex's cells move upward. The heat transfer rate enhances by increasing Rayleigh number and heated source length, while it reduces by decreasing the magnetic field effect. Some of the obtained results are consistent and in a good agreement with ones found in the literature.

Finally, the novelty of the paper can be summarized in that the proposed method provides a new efficient choice for the investigating of MHD laminar flow and heat transfer related problem. The generalizations of MOL-PACT to be applicable for handling compressible flows of low Mach number and nanofluids are of possible attention and are being pursued.

Disclosure statement

No potential conflict of interest was reported by the author(s).

ORCID

Mohamed M. Mousa http://orcid.org/0000-0001-8464-4580
Wen-Xiu Ma http://orcid.org/0000-0001-5309-1493
Mohamed R. Ali http://orcid.org/0000-0002-0795-0709

References

[1] Sharma AK, Velusamy K, Balaji C. Turbulent natural convection in an enclosure with localized heating from below. Int J Therm Sci. 2007;46:1232–1241. DOI:10.1016/j.ijthermalsci.2007.01.010

[2] Aydin O, Yang WJ. Natural convection in enclosures with localized heating from below and symmetrical cooling from sides. Int J Numer Methods Heat Fluid Flow. 2000;10:518–529. DOI:10.1108/09615530010338196

[3] Calcagni B, Marsili F, Paroncini M. Natural convective heat transfer in square enclosures heated from below. Appl Therm Eng. 2005;25:2522–2531. DOI:10.1016/j.applthermaleng.2004.11.032

[4] Deng QH, Tang GF, Li Y. A combined temperature scale for analyzing natural convection in rectangular enclosures with discrete wall heat sources. Int J Heat Mass Transf. 2002;45:3437–3446. DOI:10.1016/S0017-9310(02)00060-1

[5] Yigit S, Battu M, Turan O, et al. Free convection of power-law fluids in enclosures with partially heating from bottom and symmetrical cooling from sides. Int J Heat Mass Transf. 2019;145:118782. DOI:10.1016/j.ijheatmasstransfer.2019.118782

[6] Çolak E, Öztop HF, Ekici Ö. MHD mixed convection in a chamfered lid-driven cavity with partial heating. Int J Heat Mass Transf. 2020;156:119901. DOI:10.1016/j.ijheatmasstransfer.2020.119901

[7] Sajjadi H, Amiri Delouei A, Sheikholeslami M, et al. Simulation of three dimensional MHD natural convection using double MRT Lattice Boltzmann method. Phys A Stat Mech Appl. 2019;515:474–496. DOI:10.1016/j.physa.2018.09.164

[8] Usman M, Khan ZH, Liu MB. MHD natural convection and thermal control inside a cavity with obstacles under the radiation effects. Phys A Stat Mech Appl. 2019;535:122443. DOI:10.1016/j.physa.2019.122443

[9] Sivaraj C, Sheremet MA. MHD natural convection in an inclined square porous cavity with a heat conducting solid block. J Magn Magn Mater. 2017;426:351–360. DOI:10.1016/j.jmmm.2016.11.112

[10] Zhang JK, Li BW, Dong H, et al. Analysis of magnetohydrodynamics (MHD) natural convection in 2D cavity and 3D cavity with thermal radiation effects. Int J Heat Mass Transf. 2017;112:216–223. DOI:10.1016/j.ijheatmasstransfer.2017.04.105

[11] Shahid N, Tunç C. Resolution of coincident factors in altering the flow dynamics of an MHD elastoviscous fluid past an unbounded upright channel. J Taibah Univ Sci. 2019;13:1022–1034. DOI:10.1080/16583655.2019.1678897

[12] Schiesser WE. The numerical method of lines: integration of partial differential equations. San Diego: Academic Press; 1991.

[13] Mousa MM, Ma WX. A conservative numerical scheme for capturing interactions of optical solitons in a 2D

coupled nonlinear Schrödinger system. Indian J Phys. 2021. DOI:10.1007/s12648-021-02065-6
[14] Mousa MM. Robust schemes based on the method of lines for shock capturing. Zeitschrift Für Naturforsch A J Phys Sci. 2015;70:47–58. DOI:10.1515/ZNA-2014-0140
[15] Mousa MM. Efficient numerical scheme based on the method of lines for the shallow water equations. J Ocean Eng Sci. 2018;3:303–309. DOI:10.1016/j.joes.2018.10.006
[16] Mousa MM, Ma WX. Efficient modeling of shallow water equations using method of lines and artificial viscosity. Mod Phys Lett B. 2020;34. DOI:10.1142/S0217984920500517
[17] Alam MN, Tunç C. Constructions of the optical solitons and other solitons to the conformable fractional Zakharov–Kuznetsov equation with power law nonlinearity. J Taibah Univ Sci. 2020;14:94–100. DOI:10.1080/16583655.2019.1708542
[18] Alam MN, Tunç C. The new solitary wave structures for the $(2+1)$-dimensional time-fractional Schrodinger equation and the space-time nonlinear conformable fractional Bogoyavlenskii equations. Alexandria Eng J. 2020;59:2221–2232. DOI:10.1016/j.aej.2020.01.054
[19] Reddy JN. On penalty function methods in the finite-element analysis of flow problems. Int J Numer Methods Fluids. 1982;2:151–171. DOI:10.1002/fld.1650020204
[20] Mousa MM. Finite element investigation of stationary natural convection of light and heavy water in a vessel containing heated rods. Zeitschrift Für Naturforsch A J Phys Sci. 2012;67:421–427. DOI:10.5560/ZNA.2012-0040
[21] Mousa MM. Modeling of laminar buoyancy convection in a square cavity containing an obstacle. Bull Malaysian Math Sci Soc. 2016;39:483–498. DOI:10.1007/s40840-015-0188-z
[22] Mousa MM. Effects of porosity and heat generation on free convection in a porous trapezoidal cavity. Therm Sci. 2019;23:1801–1811. DOI:10.2298/tsci170324245m
[23] Mahmud S, Das PK, Hyder N, et al. Free convection in an enclosure with vertical wavy walls. Int J Therm Sci. 2002;41(5):440–446. DOI:10.1016/S1290-0729(02)01336-4
[24] Dukowicz JK. Computational efficiency of the hybrid penalty-pseudocompressibility method for incompressible flow. Comput Fluids. 1994;23:479–486. DOI:10.1016/0045-7930(94)90051-5
[25] Fayz-Al-Asad M, Nur Alam M, Tunç C, et al. Heat transport exploration of free convection flow inside enclosure having vertical wavy walls. J Appl Comput Mech. 2021:1–8. DOI:10.22055/JACM.2020.35381.2646
[26] Shah A, Yuan L. Numerical solution of a phase field model for incompressible two-phase flows based on artificial compressibility. Comput Fluids. 2011;42:54–61. DOI:10.1016/j.compfluid.2010.10.021
[27] Asinari P, Ohwada T, Chiavazzo E, et al. Link-wise artificial compressibility method. J Comput Phys. 2012;231:5109–5143. DOI:10.1016/j.jcp.2012.04.027
[28] Zhang JK, Dong H, Zhou EZ, et al. A combined method for solving 2D incompressible flow and heat transfer by spectral collocation method and artificial compressibility method. Int J Heat Mass Transf. 2017;112:289–299. DOI:10.1016/j.ijheatmasstransfer.2017.04.051
[29] Rouzbahani F, Hejranfar K. A truly incompressible smoothed particle hydrodynamics based on artificial compressibility method. Comput Phys Commun. 2017;210:10–28. DOI:10.1016/j.cpc.2016.09.008
[30] Temam R. Navier-Stokes equations: theory and numerical analysis. New York: Elsevier Science; 1984.
[31] Davidson PA. Introduction to magnetohydrodynamics. Cambridge University Press; 2016. DOI:10.1017/9781316672853
[32] Mousa MM. MHD free convection in a porous non-uniformly heated triangle cavity equipped with a circular obstacle subjected to various thermal configurations. Mod Phys Lett B. 2020. DOI:10.1142/s0217984920503546
[33] Isaacson E, Keller HB. Analysis of numerical methods. Dover; 2012. Available from: https://books.google.com.sa/books?id=CqPDAgAAQBAJ
[34] Ramshaw JD, Mesina GL. A hybrid penalty-pseudocompressibility method for transient incompressible fluid flow. Comput Fluids. 1991;20:165–175. DOI:10.1016/0045-7930(91)90018-D
[35] Dukowicz JK. Computational efficiency of the hybrid penalty-pseudocompressibility method for incompressible flow. Comput Fluids. 1994;23:479–486. DOI:10.1016/0045-7930(94)90051-5